Journal of Sound and Vibration 326 (2009) 671–686

Contents lists available at ScienceDirect

Journal of Sound and Vibration

journal homepage: www.elsevier.com/locate/jsvi

Vibration of isotropic and composite plates using computed shape function and its application to elastic support optimization

Jackson Kong *

Division of Building Science and Technology, City University of Hong Kong, Hong Kong

ARTICLE INFO

Article history:
Received 8 December 2008
Received in revised form
5 May 2009
Accepted 5 May 2009
Handling Editor: L.G. Tham
Available online 13 June 2009

ABSTRACT

Vibration of plates with various boundary and internal support conditions is analyzed, based on classical thin-plate theory and the Rayleigh–Ritz approach. To satisfy the support conditions, a new set of admissible functions, namely the computed shape functions, is applied to each of the two orthogonal in-plane directions. Similar to conventional finite element shape functions, parameters associated with each term of the proposed functions represent the actual displacements of the plates, thus making the method easily applicable to a wide range of support conditions, including continuous or partial edge supports and discrete internal supports. The method can also be applied to plates consisting of rectangular segments, like an L-shape plate, which sub-domains can be formulated using the computed shape functions and subsequently assembled in the usual finite element manner. Unlike many other admissible functions proposed in the literature, however, the computed shape functions presented herein are C_1—continuous and involve no complicated mathematical functions; they can be easily computed a priori by means of a continuous beam computer program and only the conventional third-order beam shape functions are involved in subsequent formulation. In all the examples given herein, only a few terms of these functions are sufficient to obtain accurate frequencies, thus demonstrating its computational effectiveness and accuracy. The method is further extended to the study of optimal location and stiffness of discrete elastic supports for maximizing the fundamental frequency of plates. Unlike rigid point supports with infinite stiffness, which optimal locations have been studied by many researchers, only discrete supports with a finite stiffness is considered in this paper. The optimal location and stiffness of discrete supports are determined for isotropic plates and laminated plates with various stacking sequences, which results are presented for the first time in literature.

1. Introduction

Vibration of isotropic and composite plates with various support conditions have been studied intensively in the past few decades, based on various plate theories, analytical and numerical methods. To date, numerical methods applied in this area can be classified into three major categories, namely (1) the finite element method including the recent meshless methods [1]; (2) the finite strip method and (3) the Rayleigh–Ritz approach using various types of admissible functions that satisfy the boundary and internal support conditions a priori. For plates without awkward geometry and relatively

* Tel.: +852 2788 9005; fax: 852 2788 9716.
E-mail address: bsjkong@cityu.edu.hk

0022-460X/$ - see front matter © 2009 Elsevier Ltd. All rights reserved.
doi:10.1016/j.jsv.2009.05.022

simple support conditions, the Ritz approach is particularly attractive in terms of its relatively rapid convergence and smaller number of unknowns, provided that an appropriate set of admissible functions can be formulated. The finite element method, on the other hand, does not require admissible functions that satisfy the support conditions a priori; support conditions are directly imposed at the corresponding nodes, thus making the method applicable to a wider range of support conditions. This advantage is attributed to the fact that, unlike many admissible functions used in the Ritz approach, the parameters associated with the shape functions of finite elements represent the actual displacements at the nodes. As such, based on the said merits of the Ritz method and the finite element method, it would be advantageous to formulate a set of admissible functions that allows support conditions to be imposed directly at nodal points of the plates, and at the same time, that converges rapidly with small number of unknowns. To this end, the proposed computed shape functions, which was previously developed by the author and Cheung [2–4] for finite strip analysis, is now modified and extended to each of the two orthogonal directions of the plates. Stiffness and mass matrices are formulated within the context of thin-plate theory using the Ritz method and the resulting eigenvalues can be easily obtained. Numerical examples of thin plates with various support conditions and non-rectangular domains are given herein to demonstrate its versatility and rapid convergence.

Extensive studies have been conducted by many researchers, particularly, for the vibration of plates with rigid point supports, because of its practical significance. Optimization of rigid point support positions for maximizing the fundamental frequencies and buckling loads of plates was studied by Xiang et al. [5], among other researchers. The maximum possible fundamental frequency was also investigated by Akesson and Olhoff [6], using the Courant maximum–minimum theorem [7]. In addition, an interesting observation was first made by Narita [8] that the natural frequencies and mode shapes can be significantly altered by adding springs of infinite stiffness (i.e. rigid point supports) at some optimal locations along the nodal lines of mode shapes. Despite a lot of studies being devoted to rigidly supported plates, it is difficult, if not impossible, to construct a support with infinite stiffness in practice, and as such, finding the optimal location for springs with a finite stiffness is of a lot more practical significance. In this respect, Won and Park [9] studied the optimal locations of elastic springs for a cantilevered isotropic plate, while Wang et al. [10] studied cantilevered isotropic plates with and without slots. Based on these previous works, elastic spring optimization of isotropic and composite plates with various boundary conditions and stacking sequences are investigated in this study using the proposed computed shape function and the direct search optimization method.

2. Computed shape functions (COMSFUN) for plate bending problems

To clarify the idea of computed shape functions, consider a typical plate strip of span L_x lying along the X-axis (Fig. 1a). The width of the strip is uniform and, for simplicity, taken as unity in the following discussion. The strip is divided into a number of beam elements, say b_e, which are not necessarily of equal length. Similar to the idea of conventional shape functions, a computed shape function is obtained by imposing a unit deflection to one of the nodes and zero deflection to the remaining nodes. The same procedure is repeated for each node and no rotation is allowed at the two ends of the beam when computing these shape functions. In addition, two other computed shape functions are obtained by imposing a unit rotation to either end of the beam while maintaining zero deflection at all nodes. As such, a total of $(b_e{+}3)$ numbers of computed shape functions can be determined.

Written in terms of the usual beam shape functions $[N(x)]$, we can express the computed shape functions as:

$$X_m(x)=\sum_{k=1}^{b_e}[N(x)]\{\alpha_m\}_k \quad \text{for } m=1,2,\ldots,p;\ \ p=b_e+3 \tag{1a}$$

where $\{\alpha_m\}_k$ denotes the nodal displacements and rotations of beam element k of the mth computed shape function $X_m(x)$. $X_1(x)$ and $X_p(x)$ correspond to the two computed shape functions with unit rotation at one end and zero rotation at the other. The remaining computed shape functions correspond to those with unit deflection at one node and zero deflection at the others.

Referring to Fig. 1b and assuming that x_n denotes the location of the nth node, the following conditions are satisfied by the COMSFUN:

For $m=2,3,\ldots p-1$

$$\begin{aligned} X_m(x_n) &= 1 \quad \text{if } m-1=n \quad \text{where } n=1,2,\ldots,p-2 \\ &= 0 \quad \text{if } m-1\neq n \end{aligned} \tag{1b}$$

and

$$\frac{dX_m(x)}{dx}=0 \quad \text{at } x=0 \quad \text{and} \quad x=L_x \tag{1c}$$

For $m=1$ or p

$$\frac{dX_1(x)}{dx}=1; \quad \frac{dX_p(x)}{dx}=0 \quad \text{at } x=0; \tag{1d}$$

$$\frac{dX_1(x)}{dx}=0; \quad \frac{dX_p(x)}{dx}=1 \quad \text{at } x=L_x; \tag{1e}$$

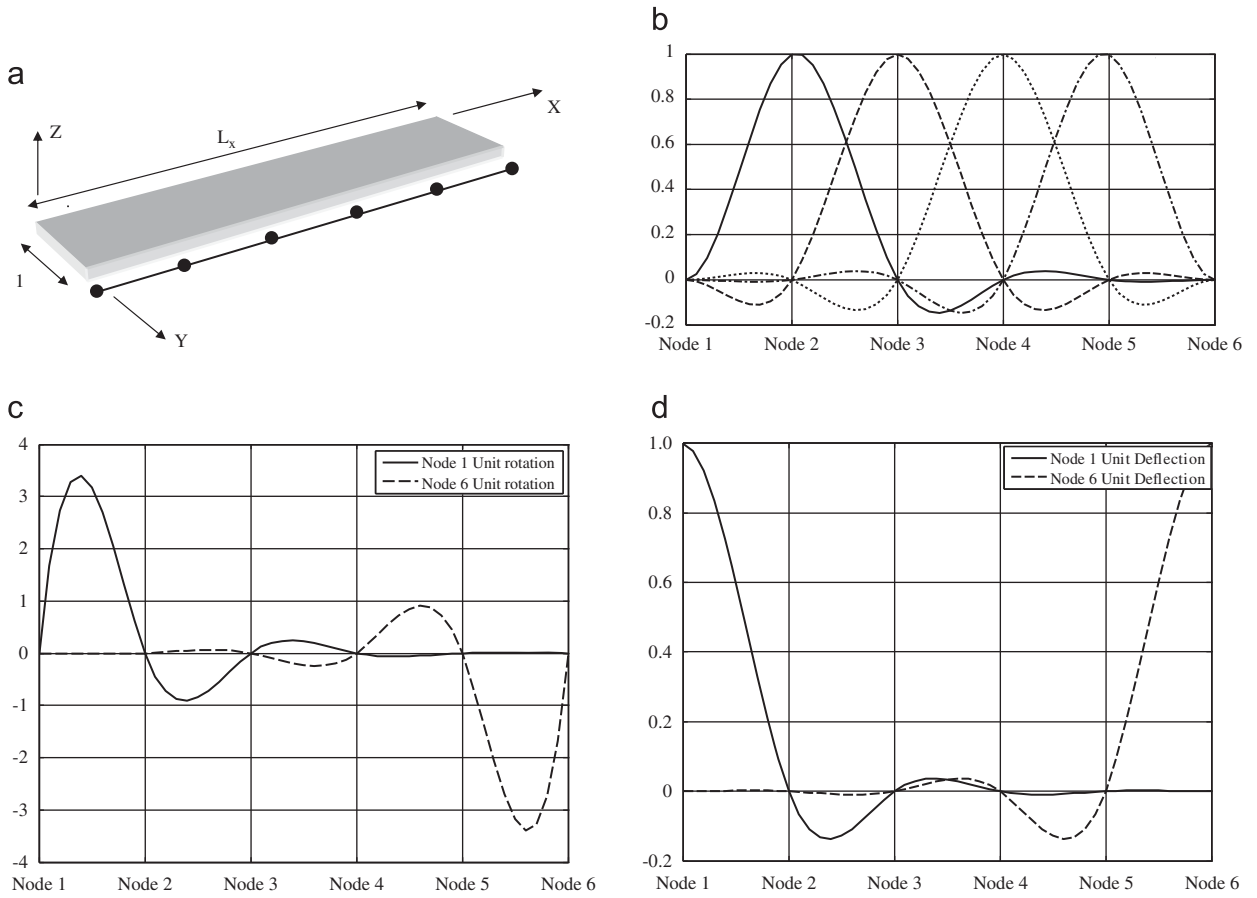

Fig. 1. (a) A plate strip is divided into five elements for computing eight shape functions; (b) computed shape functions (COMSFUN) corresponding to unit deflection at each of the interior nodes; (c) COMSFUN for unit rotation at either end (d) COMSFUN for unit deflection at either end.

and

$$X_1(x_n) = 0 = X_p(x_n) \quad \text{for all } n = 1, \ldots, p-2 \tag{1f}$$

It is apparent that the COMSFUN only comprises third-order beam functions with C_1-continuity.

For the sake of clarity, consider only the vertical (out-of-plane) displacement field at mid-plane, i.e. $w(x, y)$ of a rectangular plate segment. Using COMSFUN as the trial function in each of the two orthogonal directions, we have:

$$w(x,y) = \sum_{m}^{p} \sum_{n}^{q} X_m(x) Y_n(y) w_{mn} \tag{2}$$

where $X_m(x)$ and $Y_n(y)$ denote the mth COMSFUN and the nth COMSFUN along X- and Y-direction, respectively. p and q are the number of COMSFUN in the respective direction. The displacement parameter associated with the product $X_m(x)Y_n(y)$ is denoted by w_{mn} which represents the actual vertical displacement component or its derivatives at the corresponding nodes. To clarify the representation of the displacement parameters, a unit square plate, as shown in Fig. 2, is divided into five beam segments with eight number of computed shape functions in each direction (two for the unit rotations at the end and six for the unit nodal deflections). The displacement parameters w_{mn} of the plate segment in Fig. 2 represents (1) the vertical displacement for all interior nodes; (2) the displacement and its normal derivatives for all edge nodes and (3) the displacement and its normal and cross-derivatives for the four corner nodes. Such physical representations facilitate the direct implementation of point supports at the nodal locations.

For application to isotropic thin plates, the vertical displacement field as given by Eq. (2) can be directly applied to formulate the stiffness and mass matrices, based on thin-plate theory. In case of laminated plates with general stacking sequences (see Fig. 3), however, in-plane displacements need to be taken into account, as described in the following section.

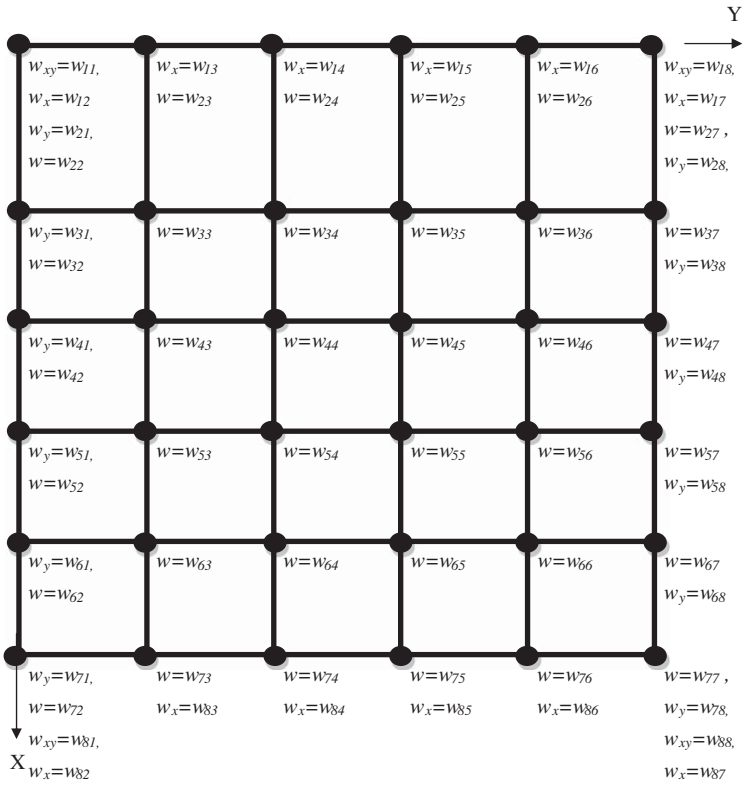

Fig. 2. Correlation between displacement parameters w_{mn} and the actual displacement and its derivatives at the nodes. w = nodal deflection; $w_x = \partial w/\partial x$ and $w_y = \partial w/\partial y$ represent the rotation about *Y*- and *X*- axis, respectively; $w_{xy} = \partial^2 w/\partial x \partial y$ denote the nodal cross-derivative (twist).

3. Stiffness and mass matrices

By neglecting transverse normal and shear deformation, the displacement field of a thin plate with thickness t can be written in terms of three independent displacement variables, that is:

$$\left.\begin{aligned} U(x,y,z) &= u(x,y) - z\frac{\partial w(x,y)}{\partial x} \\ V(x,y,z) &= v(x,y) - z\frac{\partial w(x,y)}{\partial y} \\ W(x,y,z) &= w(x,y) \end{aligned}\right\} \tag{3}$$

where $U(x, y, z)$, $V(x, y, z)$ and $W(x, y, z)$ represent the displacement of any point on the plate along the *X*-, *Y*- and *Z*-direction, respectively. Displacements on the mid-plane, i.e. $z = 0$, are denoted by $u(x, y)$, $v(x, y)$ and $w(x, y)$.

Expanding the mid-plane displacements in terms of COMSFUN gives:

$$\left.\begin{aligned} u(x,y) &= \sum_{m=1}^{p}\sum_{n=1}^{q} X_m(x)Y_n(y)u_{mn} \\ v(x,y) &= \sum_{m=1}^{p}\sum_{n=1}^{q} X_m(x)Y_n(y)v_{mn} \\ w(x,y) &= \sum_{m=1}^{p}\sum_{n=1}^{q} X_m(x)Y_n(y)w_{mn} \end{aligned}\right\} \tag{4}$$

where the w_{mn} represents the nodal out-of-plane displacement component or its derivatives, as explained in previous section and Fig. 2. Following the same representation, parameters u_{mn} and v_{mn} denote the nodal in-plane displacement components or its derivatives in the respective direction. p and q are the number of COMSFUN in the *X*- and *Y*-direction, respectively.

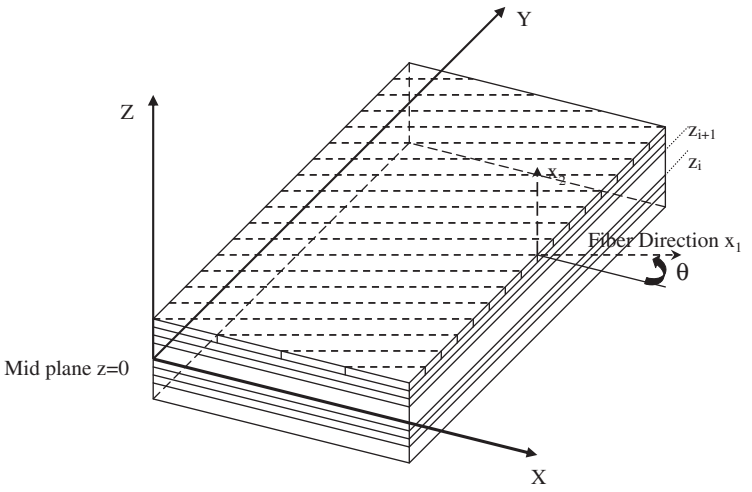

Fig. 3. A laminated composite plate with fiber direction defined by angle θ which varies from lamina to lamina. x_1 is taken as the fiber direction, x_2 being transverse to the fiber direction in the plane of the lamina. Total thickness of the plate is t. $z_0 = -t/2$ (bottom) and $z_{nL} = t/2$ (top) where nL = number of layers. $z = 0$ defines the mid-plane. For layer i, $z \in [z_i, z_{i+1}]$.

Assuming small deformation, the three in-plane strain components ε_x, ε_y and γ_{xy} can be expressed in terms of the mid-plane displacements as:

$$\{\varepsilon\} = \begin{Bmatrix} \varepsilon_x \\ \varepsilon_y \\ \gamma_{xy} \end{Bmatrix} = \begin{Bmatrix} \dfrac{\partial u(x,y)}{\partial x} \\ \dfrac{\partial v(x,y)}{\partial y} \\ \dfrac{\partial u(x,y)}{\partial y} + \dfrac{\partial v(x,y)}{\partial x} \end{Bmatrix} - z \begin{Bmatrix} \dfrac{\partial^2 w(x,y)}{\partial x^2} \\ \dfrac{\partial^2 w(x,y)}{\partial y^2} \\ 2\dfrac{\partial^2 w(x,y)}{\partial x \partial y} \end{Bmatrix} \tag{5}$$

Substituting Eq. (4) into Eq. (5) gives:

$$\{\varepsilon\} = \sum_{m=1}^{p} \sum_{n=1}^{q} [B]_{mn} \{\delta\}_{mn} \tag{6}$$

where the strain–displacement matrix $[B]_{mn}$ can be written as:

$$[B]_{mn} = \begin{bmatrix} \dfrac{dX_m}{dx} Y_n, & 0, & -z\dfrac{d^2 X_m}{dx^2} Y_n \\ 0, & X_m \dfrac{dY_n}{dy}, & -z X_m \dfrac{d^2 Y_n}{dy^2} \\ X_m \dfrac{dY_n}{dy}, & \dfrac{dX_m}{dx} Y_n, & -2z\dfrac{dX_m dY_n}{dx dy} \end{bmatrix} \tag{7}$$

and the nodal displacement vector is given by:

$$\{\delta\}_{mn} = \{u_{mn}, v_{mn}, w_{mn}\}^{\mathrm{T}}$$

For a laminated composite plate with various stacking sequence (Fig. 3), it can be shown that the stiffness and mass matrices $[K]_p^i$ and $[M]_p^i$ of layer i with density ρ_i can be written as

$$[K]_p^i = \begin{bmatrix} [K]^i_{1111} & \cdots & \cdots & [K]^i_{11pq} \\ \cdots & \cdots & \cdots & \cdots \\ \cdots & \cdots & [K]^i_{mnrs} & \cdots \\ [K]^i_{p111} & \cdots & \cdots & [K]^i_{pqpq} \end{bmatrix} \quad [M]_p^i = \begin{bmatrix} [M]^i_{1111} & \cdots & \cdots & [M]^i_{11pq} \\ \cdots & \cdots & \cdots & \cdots \\ \cdots & \cdots & [M]^i_{mnrs} & \cdots \\ [M]^i_{p111} & \cdots & \cdots & [M]^i_{pqpq} \end{bmatrix} \tag{8}$$

with

$$[K]^i_{mnrs} = \int \int \int_{z_i}^{z_{i+1}} [B]^{\mathrm{T}}_{mn} [D]_i [B]_{rs} \, dz \, dy \, dx \tag{9}$$

$$[M]^i_{mnrs} = \int \int \int_{z_i}^{z_{i+1}} [U]^{\mathrm{T}}_{mn} \rho^i [U]_{rs} \, dz \, dy \, dx, \quad z \in [z_i, z_{i+1}] \tag{10}$$

where integration is carried out for $z \in [z_i, z_{i+1}]$ of layer i with density ρ^i (see Fig. 3) and

$$[U]_{mn} = \begin{bmatrix} X_m Y_n, & 0, & -z\dfrac{dX_m}{dx}Y_n \\ 0, & X_m Y_n, & -zX_m\dfrac{dY_n}{dy} \\ 0, & 0, & X_m Y_n \end{bmatrix} \tag{11}$$

The material matrix $[D]_i$ for layer i in the global coordinate is given by:

$$[D]^i = [T]_i[d][T]_i^{\mathrm{T}} \tag{12a}$$

where $[d]_i$ is the orthotropic material matrix of layer i in the local coordinate, and $[T]_i$ is the corresponding transformation matrix [11], that is:

$$[d]_i = \begin{bmatrix} d_{11} & d_{12} & 0 \\ d_{21} & d_{22} & 0 \\ 0 & 0 & d_{66} \end{bmatrix} \tag{12b}$$

with

$$d_{11} = \frac{E_1}{1-\mu_{12}\mu_{21}}, \quad d_{12} = \frac{\mu_{12}E_2}{1-\mu_{12}\mu_{21}}, \quad d_{22} = \frac{E_2}{1-\mu_{12}\mu_{21}}, \quad d_{66} = G_{21}, \quad \mu_{21} = \mu_{12}E_2/E_1 \tag{12c}$$

and

$$[T]_i = \begin{bmatrix} \cos^2\theta_i & \sin^2\theta_i & -2\cos\theta_i \sin\theta_i \\ \sin^2\theta_i & \cos^2\theta_i & 2\cos\theta_i \sin\theta_i \\ \cos\theta_i \sin\theta_i & -\cos\theta_i \sin\theta_i & \cos^2\theta_i - \sin^2\theta_i \end{bmatrix} \tag{12d}$$

With reference to Fig. 3, the material constants E_1, E_2 represent the longitudinal modulus along the fiber direction x_1 and its transverse direction x_2, respectively. μ_{12} is the Poisson's ratio and G_{12} denotes the in-plane shear modulus. Θ_i is the inclination of fiber direction x_1 of layer i to the global X-axis.

All integration is done analytically using the software Mathematica. Summing up contributions from each layer gives the final stiffness matrix and mass matrices. It is noteworthy that the computation of $[K]^i_{mnrs}$ involves integration of the COMSFUN in each direction, which procedures are reported in [2–4].

4. Elastic support stiffness matrix

For a vertical point support with zero mass and stiffness k located at (x_s, y_s), its stiffness matrix can be written as:

$$[K_s] = k\begin{bmatrix} s_{1111} & \cdots & \cdots & s_{11pq} \\ \cdots & \cdots & \cdots & \cdots \\ \cdots & \cdots & s_{mnrs} & \cdots \\ s_{p111} & \cdots & \cdots & s_{pqpq} \end{bmatrix} = k[S] \tag{13}$$

where each term of the spring stiffness matrix $[S]$ is given by

$$s_{mnrs} = X_m(x_s)Y_n(y_s)X_r(x_s)Y_s(y_s)$$

which can be easily obtained by evaluating the respective COMSFUN $X_m(x)$ and $Y_n(y)$ at the spring location (x_s, y_s). In case the support is located directly at a node, its stiffness is directly added to the corresponding diagonal location in the plate stiffness matrix. In this study, only single or multiple supports with equal stiffness is considered, and for the latter, the total support stiffness matrix can be directly added together as:

$$[K_s] = k\sum_{i=1}^{\text{no. of springs}} [S]_i = k[S_T] \tag{14}$$

where

$$\sum_{i=1}^{\text{no. of springs}} [S]_i = [S_T]$$

It is noteworthy that the rank of $[K_s]$ is equal to the number of point supports.

5. Optimum support stiffness and location

Once the stiffness and mass matrices for plates and elastic point supports are established, the governing equation for the whole system can be written as:

$$[K_p + K_s]\{\delta\} = \omega^2[M_p]\{\delta\} \tag{15}$$

where the subscript p and s denote the plate and spring component of the system stiffness matrix and $\{\delta\}$ represents the nodal displacement vector of the system. Previous researches reveal that the frequencies of a plate can be significantly increased by adding rigid point supports (i.e. supports with infinitely large stiffness) at the optimal locations. According to the Courant–Fisher theorem [7], if m numbers of rigid point supports are added, the maximum frequency that the fundamental frequency ω_1 can be raised is bounded by the $(m+1)$th frequency (i.e. ω_{m+1}) of the original plate. As such, the optimal location of rigid point supports for maximizing the fundamental frequency of a plate is located on the nodal lines of the $(m+1)$th mode of the original plate, and the optimal location can be found by solving the following optimization problem:

$$\max \min(\omega^2(x_s, y_s))$$

$$\text{subject to } (x_s, y_s) \in \Omega_{NL} \tag{16}$$

where Ω_{NL} and (x_s, y_s) represent the nodal lines of the $(m+1)$th mode of the original plate and the locations of the additional rigid point supports, respectively. The fundamental frequency reaches its maximum value ω_{m+1}, should the optimal solutions of (16) exist.

In practice, however, it is difficult, if not impossible, to construct a support with infinite stiffness. In addition, it was shown that [9,10] the optimal location of elastic point supports varies with their stiffness. As such, in order to raise the frequencies of plates, practicing engineers would be more interested in determining the minimum support stiffness required and the corresponding optimal locations of the supports.

Assuming that it is intended to raise the fundamental frequency of a plate to the $(m+1)$th frequency ω_{m+1}, of the original plate by adding m numbers of elastic supports with the same stiffness k, one can first rearrange Eqs. (14) and (15) as:

$$[[K_p - \omega_{m+1}^2 M_p] + k[S_T]]\{\delta\} = \{0\} \tag{17}$$

which can be considered as an eigenvalue problem for the support stiffness k. Matrices on the left hand side are known quantities for given support locations. The number of positive, real and finite eigenvalues, if exist, is equal to the rank of $[K_s]$ (i.e. the number of supports, m) and the maximum of which corresponds to the minimum stiffness of the supports required to raise the fundamental frequency to the specified frequency. As such, to determine the optimal location of supports, one can minimize the support stiffness directly [9]:

$$\min max(k(x_s, y_s))$$

$$\text{subject to } (x_s, y_s) \in \Omega_{NL} \tag{18}$$

Assuming that the nodal line of vibration modes (Ω_{NL}) can be located, both optimization problems as given in (16) and (18) can be solved using direct search optimization tools available on Matlab. Based on the proposed numerical model and the direct minimization of support stiffness, optimal locations of elastic point supports are determined for isotropic and composite laminated plates with various support conditions, as given in the following examples.

5.1. Numerical examples

Examples are given below to demonstrate the application of the proposed COMSFUN to the vibration of plates and elastic support optimization of isotropic and composite laminated plates. The first two examples involve a square plate with relatively complex boundary conditions that illustrate the accuracy and convergence characteristics of the proposed method by comparing its results with those obtained using commercial finite element software (SAP and ABAQUS). Both isotropic and composite laminated plates with unsymmetric stacking sequence are given. To demonstrate its versatility, L-shape plates and a square plate with a line crack are presented in Example 3. Optimal locations of elastic point supports for isotropic cantilevered plates are presented in Example 4 and compared with results given in [10] using conventional finite elements. Extension to isotropic plates with two clamped edges is also presented, followed by composite laminated plates with various stacking sequences in Example 5.

Example 1. A square plate of isotropic material, uniform thickness and the following geometric and material properties is analyzed:

$$\text{Young's modulus} = 73.1 \times 10^9\ \text{N/m}^2;\ \text{density} = 2821\ \text{kg/m}^3;\ \text{Poisson's ratio} = 0.3;$$

$$\text{Thickness} = 0.00328\ \text{m};\ \text{length} = 0.305\ \text{m}.$$

Convergence of COMSFUN is first investigated using a plate with all edges clamped. Results are compared with FEM (using the software SAP) based on a mesh of 900 thin-plate elements, as shown in Table 1. Very good agreement can be observed between the two sets of results; with eleven numbers of COMSFUN in each direction (a total of 121 degrees of freedom), the lowest 10 frequencies can be predicted with only about 1% difference from SAP. To predict the fundamental frequency, only 7×7 numbers of COMSFUN (with 49 degrees of freedom) is sufficient to generate highly accurate result.

Based on the aforesaid convergence results, the same square plate is analyzed with different combinations of the following five types of supports:

(1) free edge (F);
(2) clamped edge (C);
(3) point supported edge (i.e. a free edge with a vertical, rigid point support at the middle);
(4) partially supported edges (P) (a free edge with half of it being free and the other half simply supported);
(5) rigid point supports.

In addition, an interesting case of a square plate with a diagonally line support is also analyzed. Frequencies obtained are compared with the analytical results and the Ritz's results of Young [14] and Abrate [15], respectively. In all cases, all supports are directly imposed at the corresponding nodes. Results in Tables 2, 3 and 6 demonstrate the accuracy of the proposed method; all results of the lowest 12 frequencies compare very favorably with the FEM results.

Example 2. To demonstrate the application to plates with membrane-bending coupling, unsymmetric cross-ply composite laminates with two layers of the following orthotropic material are analyzed:

$E_1 = 40$; $E_2 = 1$; $G_{12} = 0.2$; $\mu_{12} = 0.25$; density $= 1.0$. (refer to Eq. (12b) for definition of symbols)

Length of plate $= 100$, thickness of each layer $= 0.5$;

Fiber direction with respect to the global X-axis θ: 0/90

Results of the lowest 12 frequencies using the proposed COMSFUN ($p = q = 11$ is used which amounts to a total of 363 degrees of freedom) are first compared with ABAQUS thin-plate finite element results for two cases: either all edges simply supported or clamped. A very fine ABAQUS mesh with 2500 elements was used to accurately predict the coupling effect. In all cases, very good agreement between the two sets of results are observed from Table 4, although the COMSFUN model only involves less than 5% of the total degrees of freedom of the ABAQUS model.

The same plate is analyzed for a more complicated support condition, namely, two adjacent edges being clamped, the third edge being point-supported at the middle and the remaining edge being partially supported (half of it being free and the other half simply supported). In-plane and out-of-plane displacement components are restrained at the point support and the partially supported edge. For the clamped edge, in-plane, out-of-plane displacements and the out-of-plane rotations are restrained. Our results compare very favorably with ABAQUS's results, as shown in Table 4.

Example 3. Having established the accuracy and validity of the proposed method, L-shape cantilever plates with equal or unequal legs are used to demonstrate that the method can be extended to plates comprising rectangular segments. Each of the plates in Fig. 4 is divided into three rectangular segments, with the number of subdivision as shown thereon. For the equal-leg cantilever plate, five beam elements are used to generate eight COMSFUN in each direction for each identical

Table 1
Convergence of the first 12 frequencies (rad/s) for a square plate with all edges clamped.

Mode	FEM frequencies	COMSFUN frequencies							
	SAP	7×7[a]	Difference[b] (%)	8×8[a]	Difference[b] (%)	9×9[a]	Difference[b] (%)	11×11[a]	Difference[b] (%)
1	1948	1958	0.55	1956	0.44	1955	0.39	1955	0.36
2	3967	4041	1.86	4006	0.97	3995	0.69	3988	0.52
3	3967	4041	1.86	4006	0.97	3995	0.69	3988	0.52
4	5813	5963	2.59	5909	1.65	5892	1.36	5881	1.17
5	7111	7385	3.86	7340	3.23	7230	1.67	7166	0.77
6	7148	7409	3.65	7373	3.15	7263	1.62	7199	0.72
7	8835	9277	5.01	9147	3.53	9039	2.31	8979	1.63
8	8835	9277	5.01	9147	3.53	9039	2.31	8979	1.63
9	11 380	12 578	10.53	11 840	4.04	11 883	4.42	11 550	1.49
10	11 380			11 840	4.04	11 883	4.42	11 550	1.49
11	11 687			12 252	4.83	12 070	3.28	11 977	2.48
12	12 944			13 639	5.37	13 582	4.93	13 257	2.42

For the case with 7×7 terms of COMSFUN, only nine active degrees of freedom remains after applying the support conditions.

[a] Number of terms used for COMSFUN $= p \times q$.

[b] Percentage difference from the SAP results.

Table 2
First 12 frequencies (rad/s) for a square plate with various supports.

Mode	1	2	3	4	5	6	7	8	9	10	11	12
CFFF[a]												
SAP	188.20	458.85	1147.10	1464.80	1663.50	2894.50	3299.60	3434.00	3794.00	4944.70	5163.40	6366.70
COMSFUN	188.61	462.23	1156.47	1477.27	1682.05	2944.22	3329.29	3485.18	3857.87	5051.23	5276.66	6486.91
Difference (%)	0.22	0.74	0.82	0.85	1.11	1.72	0.90	1.49	1.68	2.15	2.19	1.89
CCFF[a]												
SAP	375.08	1290.30	1437.80	2564.40	3376.80	3534.40	4586.00	4739.20	6516.50	6666.50	6842.60	7704.80
COMSFUN	374.28	1290.21	1443.01	2577.46	3400.14	3549.06	4632.95	4799.20	6581.17	6741.94	6971.26	7858.59
Difference (%)	−0.21	−0.01	0.36	0.51	0.69	0.41	1.02	1.27	0.99	1.13	1.88	2.00
CCCF[a]												
SAP	1297.10	2156.40	3428.50	4119.90	4338.50	6231.80	6628.20	7200.30	7548.00	9178.90	9415.10	10 892.00
COMSFUN	1281.49	2156.60	3391.75	4158.16	4340.44	6308.69	6576.41	7315.89	7574.43	9387.99	9563.75	10 900.81
Difference (%)	1.20	−0.01	1.07	−0.93	0.04	1.23	0.78	1.61	0.35	2.28	1.58	0.08
CCCP[a]												
SAP	1707.90	3256.10	3428.50	4338.50	5230.10	6231.80	6846.10	7411.00	8742.80	9178.90	10 421.00	10 892.00
COMSFUN	1713.97	3265.91	3391.75	4340.44	5201.12	6308.69	6867.94	7464.72	8905.44	9387.99	10 574.65	10 900.81
Difference (%)	0.36	0.30	−1.07	0.04	−0.55	1.23	0.32	0.72	1.86	2.28	1.47	0.08
CCCS[a]												
SAP	1713.40	3284.20	3767.90	4728.30	5829.10	6757.80	7125.10	8402.00	8915.90	10 404.00	11 121.00	11 300.00
COMSFUN	1718.94	3282.82	3770.00	4681.65	5872.64	6782.21	7181.04	8514.94	9086.69	10 537.75	11 299.78	11 498.15
Difference (%)	0.32	−0.04	0.06	−0.99	0.75	0.36	0.79	1.34	1.92	1.29	1.61	1.75
CCCS+PS[b]												
SAP	3006.20	3764.40	4135.20	4798.80	6058.40	6784.40	8300.10	8786.30	9886.90	10 429.00	11 244.00	12 068.00
COMSFUN	3014.19	3765.06	4194.58	4764.40	6100.53	6815.50	8417.28	8949.79	10 192.20	10 568.96	11 370.79	12 221.58
Difference (%)	0.27	0.02	1.44	−0.72	0.70	0.46	1.41	1.86	3.09	1.34	1.13	1.27

[a] C = clamped edge; F = free edge; S = partially supported edge; P = point-supported edge. CCFF = two adjacent edges clamped and the remaining two free.
[b] CCCS+PS = CCCS and a point support at the center of the plate. Number of terms used for COMSFUN = 11×11 in all cases.

Table 3
First 12 frequencies for a square plate with various supports.

Mode	1	2	3	4	5	6	7	8	9	10	11	12
CCCP*												
SAP	1707.90	3256.10	3428.50	4338.50	5230.10	6231.80	6846.10	7411.00	8742.80	9178.90	10 421.00	10 892.00
COMSFUN	1713.97	3265.91	3391.75	4340.44	5201.12	6308.69	6867.94	7464.72	8905.44	9387.99	10 574.65	10 900.81
Difference (%)	0.36	0.30	−1.07	0.04	−0.55	1.23	0.32	0.72	1.86	2.28	1.47	0.08
CCCS*												
SAP	1713.40	3284.20	3767.90	4728.30	5829.10	6757.80	7125.10	8402.00	8915.90	10 404.00	11 121.00	11 300.00
COMSFUN	1718.94	3282.82	3770.00	4681.65	5872.64	6782.21	7181.04	8514.94	9086.69	10 537.75	11 299.78	11 498.15
Difference (%)	0.32	−0.04	0.06	−0.99	0.75	0.36	0.79	1.34	1.92	1.29	1.61	1.75
CCCS+Pt Supp[a]												
SAP	3006.20	3764.40	4135.20	4798.80	6058.40	6784.40	8300.10	8786.30	9886.90	10 429.00	11 244.00	12 068.00
COMSFUN	3014.19	3765.06	4194.58	4764.40	6100.53	6815.50	8417.28	8949.79	10 192.20	10 568.96	11 370.79	12 221.58
Difference (%)	0.27	0.02	1.44	−0.72	0.70	0.46	1.41	1.86	3.09	1.34	1.13	1.27

* C = clamped edge; S = partially supported edge; P = point-supported edge. CCCS = three adjacent edges clamped and the remaining one partially supported.
[a] CCCS and one point support at the center of the plate. Number of terms used for COMSFUN = 11×11 in all cases.

segment; for the unequal-leg cantilever plate, however, different numbers of COMSFUN are used in each segment provided that compatibility is maintained across the interface. Stiffness and mass matrices for each segment are formed and they are then assembled for the entire plate in the conventional finite element manner, while maintaining compatibility of deflection and slope across the interfaces. As shown in Fig. 4, the plate is clamped on one edge with or without point supports, and the lowest 10 frequencies are compared with ABAQUS using a fine mesh of 1200 elements. In all cases, the COMSFUN results agree closely with the ABAQUS results with less than 1.5% difference, as shown in Table 5.

Another interesting problem involves a simply supported plate with a line crack along its center line, see Fig. 5. Due to symmetry, half of the plate is analyzed using COMSFUN. Rotations and vertical deflections are restrained along the

Table 4
First 12 frequencies ($\times 10^{-3}$ rad/s) for an un-symmetric cross-ply square plate with different support conditions.

Mode	1	2	3	4	5	6	7	8	9	10	11	12
SSSS												
COMSFUN	1.5749	3.2011	3.2011	4.3665	7.2745	7.2912	7.9529	7.9529	10.4500	12.1320	12.1320	12.6562
ABAQUS	1.5755	3.2033	3.2033	4.3681	7.2527	7.2692	7.9298	7.9298	10.4077	11.9058	11.9058	12.4298
Difference (%)	−0.04	−0.07	−0.07	−0.04	0.30	0.30	0.29	0.29	0.41	1.90	1.90	1.82
CCCC												
COMSFUN	2.3721	4.9204	4.9204	6.6088	9.2768	9.2844	10.3420	10.3420	13.1287	15.6741	15.6741	16.3738
ABAQUS	2.3737	4.9222	4.9222	6.6081	9.2123	9.2199	10.2788	10.2788	13.0228	15.0964	15.0964	15.8129
Difference (%)	−0.07	−0.04	−0.04	0.01	0.70	0.70	0.61	0.61	0.81	3.83	3.83	3.55
CCSP												
COMSFUN	1.0451	1.8609	3.7902	4.0741	4.8298	5.5337	6.6031	7.0491	8.5697	9.2349	9.9785	10.2045
ABAQUS	1.0320	1.8355	3.6969	4.0355	4.7696	5.4720	6.4928	6.9176	8.5279	9.1370	9.8978	10.0656
Difference (%)	1.21	1.38	2.52	0.96	1.26	1.13	1.70	1.90	0.49	1.07	0.81	1.38

Number of terms used for COMSFUN $= 11 \times 11$ in all cases.

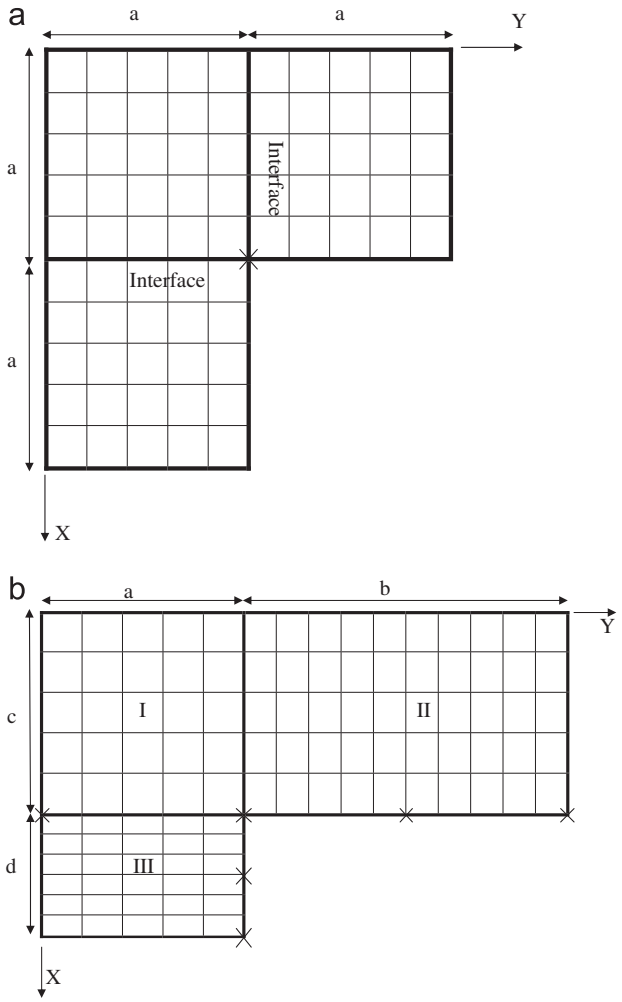

Fig. 4. (a) An equal-leg L-shape plate divided into three identical square segments. $a = 100$ units. Continuity of slope and deflection are maintained across their interfaces. $p = q = 8$ for each segment. (b) An unequal leg L-shape plate with three unequal rectangular segments. $a = c = 100$, $b = 160$, $d = 60$. $p = q = 8$ for segment I, $p = 8$, $q = 13$ for segment II, $p = 9$, $q = 8$ for segment III. The plates are clamped at $X = 0$ with or without point supports, which are denoted by X in the figure. $E = 40$; $\mu = 0.25$; density $= 1$; thickness $= 1$.

Table 5
First 10 frequencies ($\times 10^{-3}$ rad/s) for L-shape cantilevered plates in Fig. 4.

Mode	1	2	3	4	5	6	7	8	9	10
Equal-leg cantilever Fig. 4(a)										
COMSFUN	0.1992	0.7331	0.9654	1.3117	2.3450	2.9051	3.7156	4.3150	4.7060	5.0101
ABAQUS	0.1989	0.7321	0.9625	1.3057	2.3411	2.9060	3.7062	4.3116	4.6826	5.0032
Difference (%)	0.16	0.13	0.31	0.46	0.17	0.03	0.26	0.08	0.50	0.14
Equal-leg cantilever+one point support Fig. 4(a)										
COMSFUN	0.3074	0.8972	1.1876	1.7536	2.9022	3.4933	3.7251	4.5602	4.8398	5.0190
ABAQUS	0.3059	0.8949	1.1787	1.7440	2.9020	3.4638	3.7127	4.5368	4.8187	5.0091
Difference (%)	0.49	0.26	0.75	0.55	0.01	0.85	0.33	0.51	0.44	0.20
Unequal-leg cantilever Fig. 4(b)										
COMSFUN	0.2431	0.7583	1.1276	1.6097	2.3402	3.9585	4.4107	4.9566	5.2842	6.0391
ABAQUS	0.2422	0.7516	1.1176	1.5922	2.3102	3.9060	4.3627	4.8872	5.2168	5.9524
Difference (%)	0.41	0.88	0.90	1.10	1.30	1.13	1.11	1.42	1.29	1.46
Unequal-leg cantilever+six point supports Fig. 4(b)										
COMSFUN	2.1749	2.7185	3.2968	3.3877	4.8249	5.1455	5.8749	6.5667	7.3726	8.6545
ABAQUS	2.1643	2.7197	3.2645	3.3624	4.7586	5.0817	5.8059	6.4704	7.2629	8.5354
Difference (%)	0.49	0.04	0.99	0.75	1.39	1.25	1.19	1.49	1.50	1.40

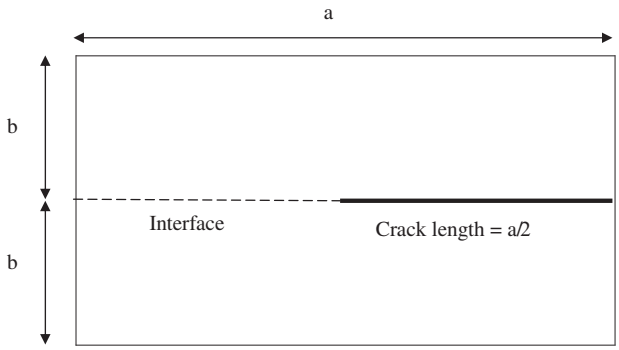

Fig. 5. A rectangular plate with a central line crack.

Table 6
First five frequencies parameters $\lambda^2 = \omega a^2 (\rho t/D)^{1/2}$ for an isotropic square plate with simply-supported edges and a diagonally line support. Number of terms used for COMSFUN = 11×11.

	Frequency λ^2		
Mode	COMSFUN	Abrate [15]	Analytical [14]
1	50.015	49.3480	49.348
2	66.432	66.020	65.80
3	100.095	98.696	98.696
4	121.708	122.552	121.95
5	129.886	128.305	128.300

separation line for the symmetric modes and anti-symmetric modes, respectively. In both cases, the crack line remains free. COMSFUN results are compared with analytical results [12,13] and good agreement among the three sets of results can be observed from Table 7.

Example 4. The isotropic square plate as given in Example 1 is analyzed again with elastic spring supports. Only one of the edges is fully clamped with the remaining edges free. This plate was previously studied by Wang et al. [10] for support optimization. The first three fundamental frequencies obtained using COMSFUN are compared with Wang's FEM results, and excellent agreement can be observed from Table 8. The second mode of this cantilever plate corresponds to a torsional mode about its axis of symmetry (see Fig. 6). As such, an elastic support is placed at the center of the free edge opposite to the clamped edge, and its minimum stiffness required to raise the fundamental frequency to the second frequency of the original plate (ω_2) is determined by using the eigenvalue Eq. (17). The minimum stiffness obtained using the COMSFUN

Table 7
Comparison of normalized frequencies $\lambda^2 = \omega a^2 (\rho t/D)^{1/2}$ for the first three anti-symmetric and symmetric modes of a cracked plate.

Modes	COMSFUN[a]	Yu [13]	Stahl et al. [12]	Difference (%)
A1	72.02	73.43	73.52	2.04
A2	169.61	168.6	168.6	−0.60
A3	196.87	197.9	198	−0.57
S1	41.90	40.46	40.32	3.92
S2	72.72	72.78	72.77	−0.07
S3	124.20	123.5	123.5	−0.56

$D = Et^3/12(1-\mu^2)$.

[a] COMSFUN used: symmetric half of the plate was analyzed with $p = 7$ along the shorter span and $q = 11$ along the direction of the cracked center line.

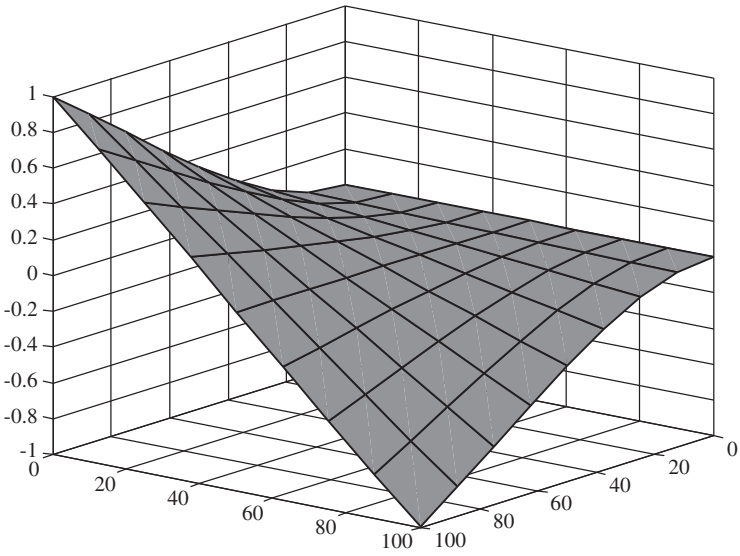

Fig. 6. Second mode of a cantilever (CFFF) plate.

Table 8
Comparison of frequencies (Hz), minimum support stiffness ($k_s L^2/D$) and the corresponding support location (x/L for cantilever 2 or y/L for cantilever 3) for a cantilevered square plate with $L = 0.305$ m. The plate is clamped at $x = 0$. $D = Et^3/12(1-\mu^2)$.

	Frequency			
Mode	COMSFUN	Wang [10]	Difference (%)	
1	30.018	30.005	0.04	
2	73.566	73.555	0.02	
3	184.058	184.394	−0.18	
	Support stiffness		Support Location	
Problem[a]	COMSFUN	Wang [10]	COMSFUN	Wang [10]
Cantilever 1	24.08951	23.96060		
Cantilever 2	23.69508	23.63130	0.97071	0.97340
Cantilever 3	9.32034	9.32620	0.28993	0.28400

[a] cantilever 1 = point support located at the middle of the free edge (i.e. at $x/L = 1$, $y/L = 0.5$); cantilever 2 = support located along the axis of symmetry (i.e. along $y/L = 0.5$); cantilever 3 = two supports located symmetrically about the center of the free edge (i.e. they are located along $x/L = 1$). Number of terms used for COMSFUN = 11×11.

model agrees very well with Wang's FEM model, see Table 8 (cantilever 1). This location, however, does not correspond to the optimal location. On this axis of symmetry, positive eigenvalue of Eq. (17) does not exist for supports located from the clamped edge up to $x = 0.1525$ m, thus indicating that even a rigid support located within this region is unable to raise the fundamental frequency to ω_2. A plot of the minimum support stiffness required, from $x = 0.25$ m up to the free edge, is given in Fig. 7, which clearly shows that the optimum location is located close to the free edge, but not exactly thereon. The final optimum location and the corresponding minimum support stiffness are given in Table 8 (cantilever 2), which compare well with Wang's findings.

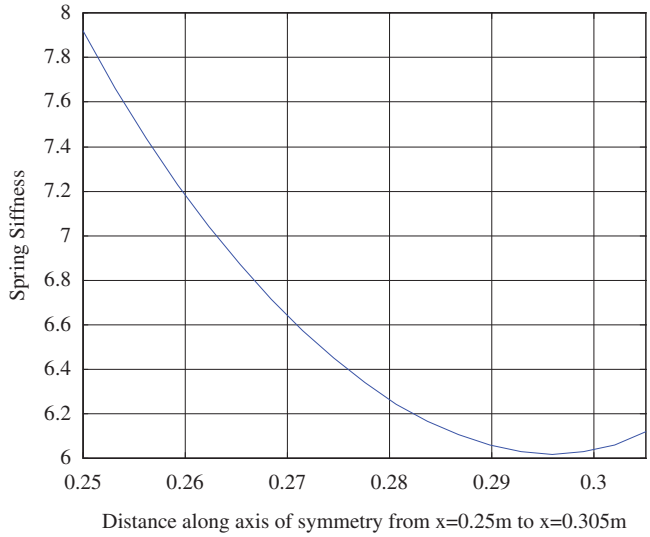

Fig. 7. Variation of minimum spring support stiffness ($\times 10^4$ N/m) along the axis of symmetry of the cantilever plate.

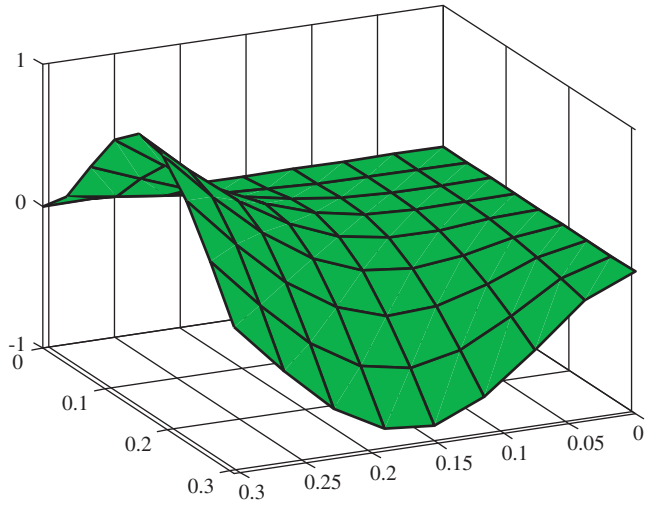

Fig. 8. Second mode of a plate with two adjacent edges clamped and the remaining edges free.

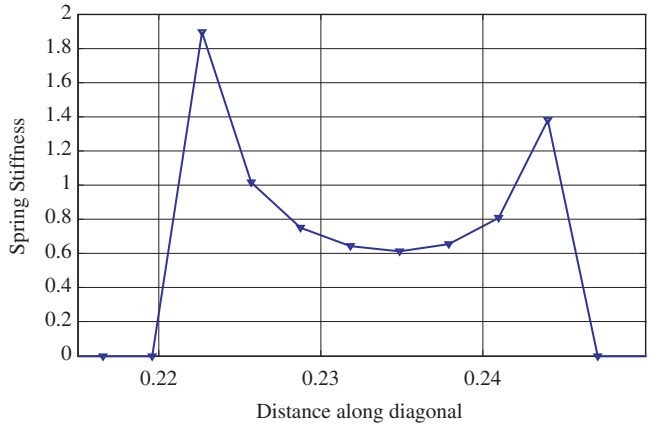

Fig. 9. Variation of minimum spring support stiffness ($\times 10^6$ N/m) along the diagonal ($x\sqrt{2}$) of the CCFF plate.

Alternatively, to raise the fundamental frequency of the cantilevered plate to ω_2, two elastic supports are placed symmetrically along the free edge. The optimal locations of the supports are obtained directly by minimizing the support stiffness. Our results compare favorably with those of Wang, as indicated in Table 8 (cantilever 3).

Table 9
Minimum support stiffness (k_sL^2/D) for simply supported, composite laminates.

Antisymmetric angle-ply				Unsymmetric unbalanced laminate			
	Frequency[a]				Frequency[a]		
Angle	Mode 1 ω_1	Mode 2 ω_2	Support stiffness	Angle	Mode 1 ω_1	Mode 2 ω_2	Support stiffness
90/90	1.8543	2.2303	16.1952	0/90	1.5749	3.2011	91.2621
75/−75	1.6570	2.3847	31.0737	0/75	1.5745	3.0582	75.6899
60/−60	1.7291	3.1285	95.4378	0/60	1.6030	2.8975	63.9214
45/−45	1.8389	3.7296	257.1598	0/45	1.6466	2.7319	51.9092
30/−30	1.7291	3.1285	95.4378	0/30	1.6500	2.4957	35.9773
15/−15	1.6570	2.3847	31.0737	0/15	1.7328	2.2761	22.6669
0/0	1.8543	2.2303	16.1952	0/0	1.8543	2.2303	16.1952

$L = 100$; $D = E_1t^3/12(1-\mu_{12}^2)$.
[a] First two natural frequencies ($\times 10^{-3}$ rad/s) of the original plate.

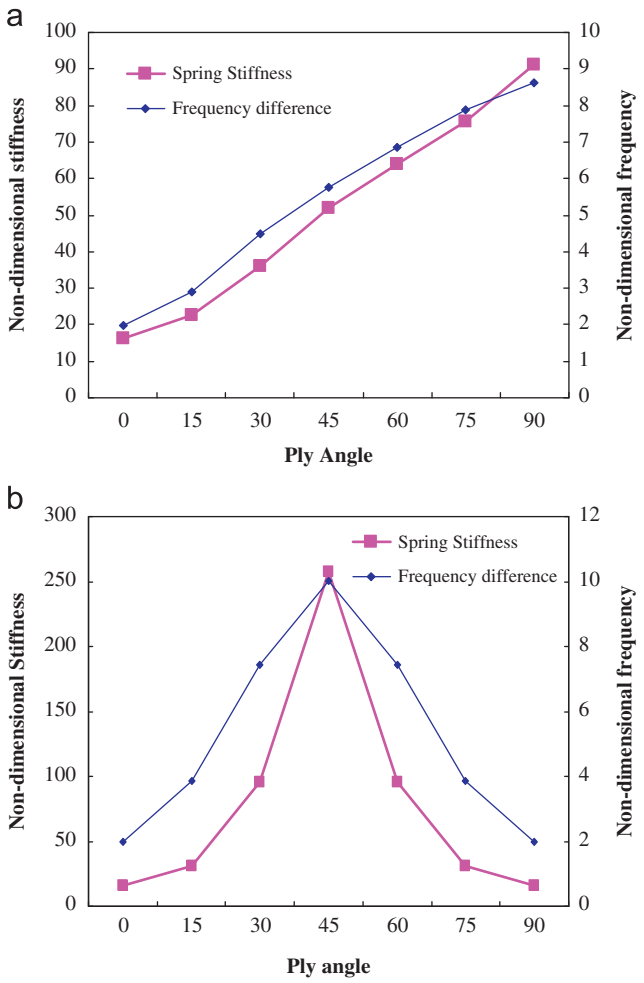

Fig. 10. Variation of non-dimensional spring support stiffness (k_sL^2/D) and differences in non-dimensional frequency $(\omega_2-\omega_1)L^2(\rho t/D)^{0.5}$ against the ply angle (θ in degree) for (a) unbalanced, unsymmetric laminates ($0/\theta$); (b) anti-symmetric angle-ply laminates ($\theta/-\theta$). $L = 100$; $\rho = 1$, $D = E_1t^3/12(1-\mu_{12}^2)$.

The same isotropic square plate is analyzed again with two adjacent edges fully clamped and the remaining edges free. Unlike the previous case, the second mode of this plate corresponds to a torsional mode about its diagonal, as shown in Fig. 8. A plot of the minimum support stiffness along the diagonal indicates that the optimum location can only be found in the region as shown in Fig. 9, beyond which positive eigenvalues of Eq. (17) does not exist. By directly minimizing the support stiffness, the exact location of $x = 0.2347$ m, $y = 0.2347$ m on the diagonal and the corresponding minimum spring stiffness of $k_s L^2/D = 241.5082$ can be found. In this case, no result is available in the literature for comparison.

Example 5. A two-layer, composite laminated square plate with geometry and material properties being the same as those defined in Example 2 is analyzed. In addition to unsymmetric cross-ply laminates, anti-symmetric angle-ply $(\theta/-\theta)$ and unsymmetric, unbalanced $(0/\theta)$ laminates are also considered. The plate is simply supported around all edges with both in-plane and out-of-plane displacements being restrained. An elastic spring is imposed at the center of the plate and the objective is to determine its minimum stiffness required to raise the fundamental frequency of the supported plate to the second natural frequency of the original plate. Results for both cases are summarized in Table 9 and Fig. 10, which clearly demonstrates that the variation of minimum spring stiffness required for various ply angles follows closely the corresponding change in frequency $(\omega_2 - \omega_1)$ required.

6. Conclusions

Vibration of isotropic and composite laminated plates with various boundary and internal support conditions is analyzed in a unified manner using the computed shape function and thin-plate theory. Similar to the conventional finite element shape functions, parameters associated with each term of the proposed functions represent the actual displacements of the plates, thus making the method easily applicable to a wide range of support conditions, as demonstrated in the examples given. The method is also applied to analyze L-shape plates, which can be sub-divided into rectangular segments and assembled in the usual finite element manner. It is noteworthy that, unlike other admissible functions proposed in the literature, the computed shape functions presented herein are C_1—continuous and involve no complicated mathematical functions or implementation. In all the given examples, only several terms of these functions are sufficient to obtain very accurate results for the lowest 10 frequencies, thus demonstrating its computational effectiveness and rapid convergence.

Taking advantage of the computational efficiency of the proposed method, it is also applied to determine the optimal location and stiffness of discrete elastic supports in maximizing the fundamental frequency of isotropic plates and composite plates. For isotropic plates with one edge clamped, the minimum stiffness and optimal locations determined are verified against available results from the literature. In addition, the method was used to analyze plates with two adjacent clamped edges and also simply supported composite plates with various stacking sequences; no results are available in the literature for comparison in these cases. In this study, only examples of plates that allow easy location of the nodal lines are given; the method is currently being extended to general cases where the nodal lines of vibration cannot be easily identified.

Acknowledgement

The work described in this paper was fully supported by a grant from City University of Hong Kong (Project no. 7001774).

References

[1] Y. Chen, J.D. Lee, A. Eskandarian, *Meshless Methods in Solid Mechanics*, Springer, New York, NY, 2006.
[2] Y.K. Cheung, J. Kong, A new finite strip for analyzing deep beams and shear walls, *Communications in Numerical Methods in Engineering* 11 (1995) 643–653.
[3] Y.K. Cheung, J. Kong, The application of a new finite strip to the free vibration of rectangular plates of varying complexity, *Journal of Sound and Vibration* 181 (2) (1995) 341–353.
[4] Y.K. Cheung, J. Kong, Vibration and buckling of thin-walled structures by a new finite strip, *Thin-Walled Structures* 21 (4) (1995) 327–343.
[5] Y. Xiang, C.M. Wang, S. Kitipornchai, Optimal locations of point supports in plates for maximum fundamental frequency, *Structural Optimization* 11 (3/4) (1996) 170–177.
[6] B. Akesson, N. Olhoff, Minimum stiffness of optimally located supports for maximum value of beam eigenfrequencies, *Journal of Sound and Vibration* 120 (1988) 457–463.
[7] R. Courant, D. Hilbert, *Methods of Mathematical Physics*, Vol. 1, Interscience, New York, 1953.
[8] Y. Narita, The effect of point constraints on transverse vibration of cantilever plates, *Journal of Sound and Vibration* 102 (1985) 305–313.
[9] K.M. Won, Y.S. Park, Optimal Support positions for a structure to maximize its fundamental natural frequency, *Journal of Sound and Vibration* 213 (5) (1998) 801–812.
[10] M.I. Friswell, D. Wang, The minimum support stiffness required to raise the fundamental natural frequency of plate structures, *Journal of Sound and Vibration* 301 (2007) 665–677.
[11] J.N. Reddy, *Mechanics of Laminated Composite Plates and Shells: Theory and Analysis*, CRC Press, Boca Raton, FL, 2004.
[12] B. Stahl, L.M. Keer, Vibration and Stability of cracked rectangular plates, *International Journal of Solids and Structures* 8 (1972) 69–91.

[13] W.L. Cleghorn, S.D. Yu, J.S. Xu, R.G. Fenton, Free vibration analysis of rectangular plates with a linear crack along the central axis, *Proceedings of the ASME Winter Annual Meeting*, Chicago, IL, November 5–11, 1994.
[14] P.G. Young, S.M. Dickinson, On the free flexural vibration of rectangular plates with straight or curved internal line supports, *Journal of Sound and Vibration* 162 (1) (1993) 123.
[15] S. Abrate, Vibration of composite plates with internal supports, *Journal of Mechanical Science* 36 (11) (1994) 1027–1043.